Electronic Supplementary Information

for

Multi-functional MnO_2 nanomaterials for photo-activated applications by a plasma-assisted fabrication route

Davide Barreca,*[a] Filippo Gri,[b] Alberto Gasparotto,[b] Giorgio Carraro,[b] Lorenzo Bigiani,[b] Thomas Altantzis,[c] Bostjan Zener,[d] Urška Lavrenčič Štangar,[d,e] Bruno Alessi,[f] Dilli Babu Padmanaban,[f] Davide Mariotti[f] and Chiara Maccato*[b]

[a] *CNR-ICMATE and INSTM, Department of Chemical Sciences, Padova University, Via Marzolo 1, 35131 Padova, Italy*

[b] *Department of Chemical Sciences, Padova University and INSTM, Via Marzolo 1, 35131 Padova, Italy*

[c] *EMAT, University of Antwerp, 2020 Antwerp, Belgium*

[d] *Faculty of Chemistry and Chemical Technology, University of Ljubljana, 1000 Ljubljana, Slovenia*

[e] *Laboratory for Environmental and Life Sciences, University of Nova Gorica, 5000 Nova Gorica, Slovenia*

[f] *Nanotechnology & Integrated Bio-Engineering Centre (NIBEC), Ulster University, BT37 0QB, UK*

* Corresponding authors. E-mail: davide.barreca@unipd.it; chiara.maccato@unipd.it

§ S-1. Characterization

§ S-1.1 X-ray photoelectron spectroscopy (XPS)

The surface C1s signal (Fig. S1) could be fitted by means of four distinct components. Bands (I) and (II), centered at BE = 284.8 eV and 286.3 eV, respectively, were attributed to adventitious carbon contamination and to surface C-O moieties.[1, 2] The two components located at 289.0 eV (III) and 292.6 eV (IV) were mainly ascribed to CF and CF_2 residuals from the used Mn precursor.[3] The surface C1s photopeak was reduced to noise level after Ar^+ erosion for 5 min, indicating thus that carbon presence was limited to the sample surface and highlighting the purity of the obtained systems.

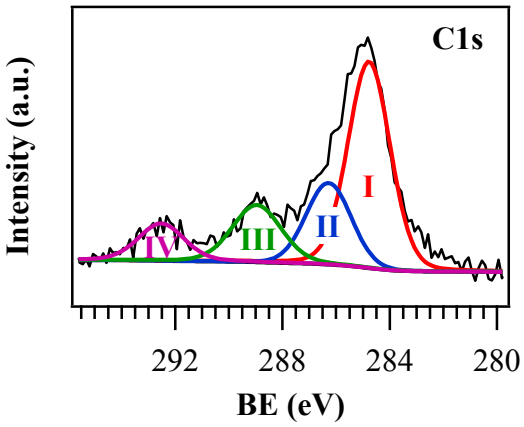

Figure S1. Surface C1s photopeak for a manganese oxide specimen grown at 200 °C.

§ S-1.2 Energy dispersive X-ray spectroscopy (EDXS)

EDXS compositional analyses were carried out both in plane and in cross-sectional mode. Fig. S2a reports a representative spectrum, in which O, Mn and F signals could be clearly discerned. Na, Si and Sn signals originate from the growth substrate. Cross-sectional analyses (Fig. S2b) evidenced an almost parallel distribution of O, Mn and F throughout the deposit, suggesting their common chemical origin and demonstrating a uniform in-depth fluorine distribution.

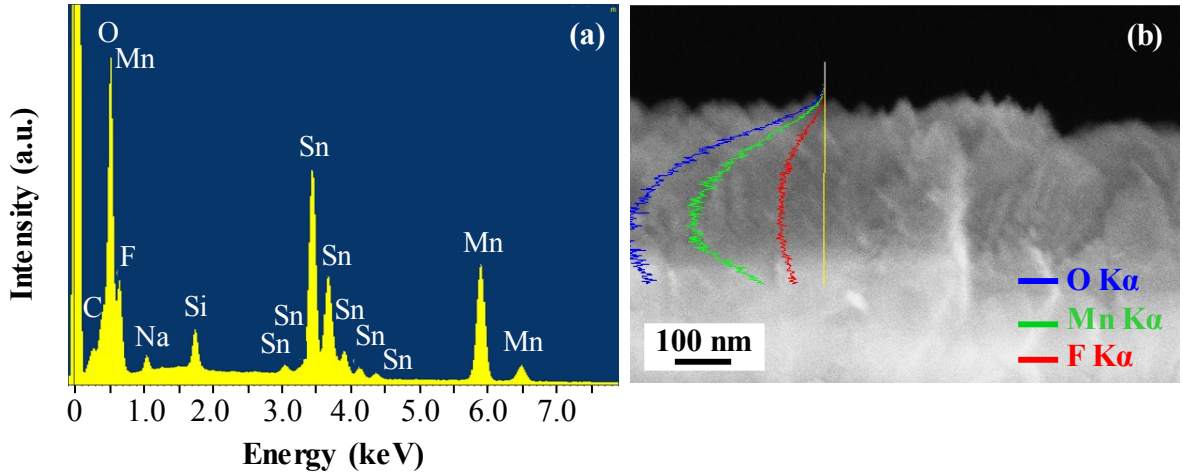

Figure S2. (a) EDXS spectrum for a manganese oxide sample deposited at 200 °C. (b) Cross-sectional EDXS O Kα, Mn Kα and F Kα line-scans for the same specimen.

§ S-1.3 Atomic force microscopy (AFM)

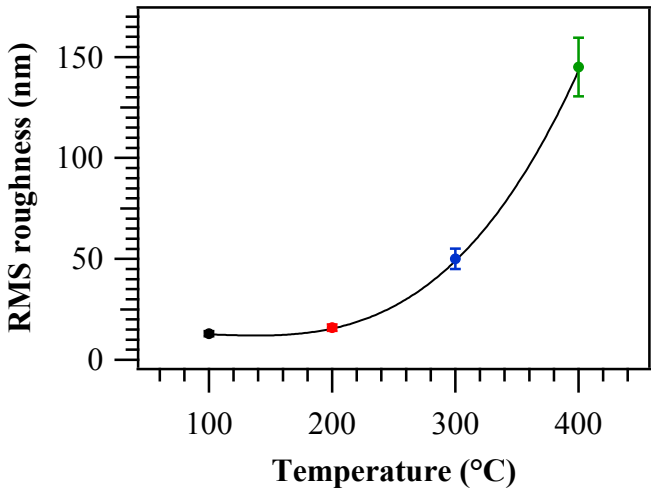

Figure S3. Evolution of the root mean square (RMS) roughness obtained by AFM measurements as a function of the adopted deposition temperature.

§ S-1.4 Kelvin probe (KP) and valence band XPS results

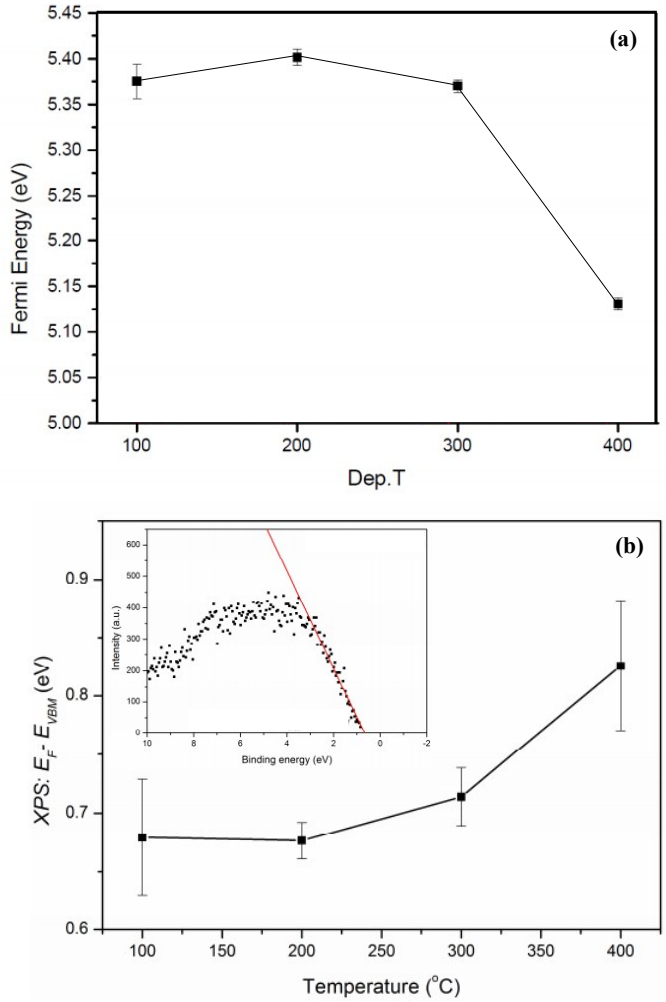

Figure S4. (a) Absolute Fermi energy obtained by KP. (b) Valence band onset with respect to the Fermi level as determined by XPS valence band measurements. In the inset, experimental data for the sample grown at 200° C are provided as an example.

§ S-1.5 Photocatalytic tests

The photocatalytic activity mechanism leading to the degradation of the target dye can be described as follows:[4-9]

$MnO_2 + h\nu \rightarrow MnO_2(e^-) + h^+$ (S1)

$h^+ + H_2O \rightarrow HO^\bullet$ (S2)

$e^- + O_2 \rightarrow O_2^{\bullet-}$ (S3)

$O_2^{\bullet-} + H_2O \rightarrow HO_2^\bullet + HO^\bullet$ (S4)

$O_2^{\bullet-}$/ $HO^\bullet$ / $HO_2^\bullet$ + organic pollutant $\rightarrow$ degradation products (S5)

Upon irradiation of the catalyst, holes (h^+) and electrons (e^-) are simultaneously generated in its valence and conduction bands, respectively [equation (S1)]. Subsequently, holes reaction with water molecules results in the formation of hydroxyl radicals [equation (S2)]. In turn, photogenerated electrons can be scavenged by dissolved O_2, yielding superoxide radical anions and generate $HO_2^\bullet$ and $HO^\bullet$ species [equations (S3) and (S4)]. Finally, the target organic pollutant can be effectively oxidized by the photogenerated radicals, generating mineralized products (CO_2, H_2O,…) [equation (S5)] .

	k **(min^{-1})**	**$t_{1/2}$ (min)**
UV irradiation	(0.025±0.001)	28
Vis irradiation	(0.022±0.002)	31

Table S1. Comparison of first-order reaction rate constants and half-life times for the photobleaching of Plasmocorinth B solutions under UV and Vis illumination for a β-MnO_2 specimen deposited at 200 °C.

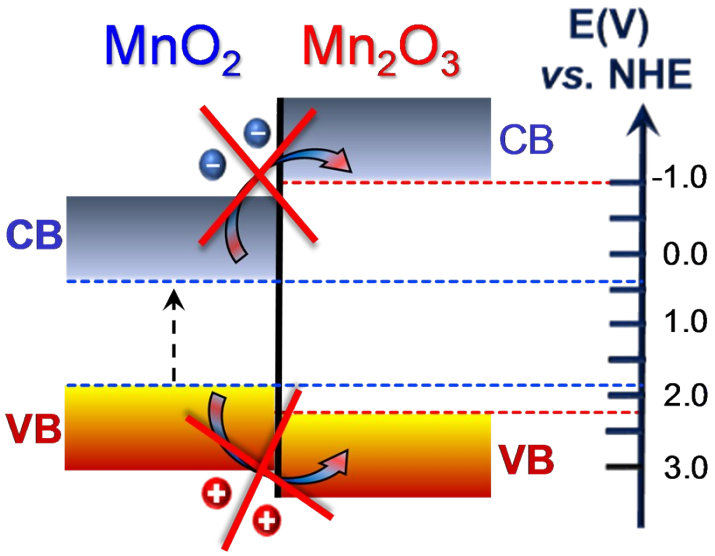

Figure S5. Schematic representation of the band structures of β-MnO_2 and cubic Mn_2O_3 [10, 11].

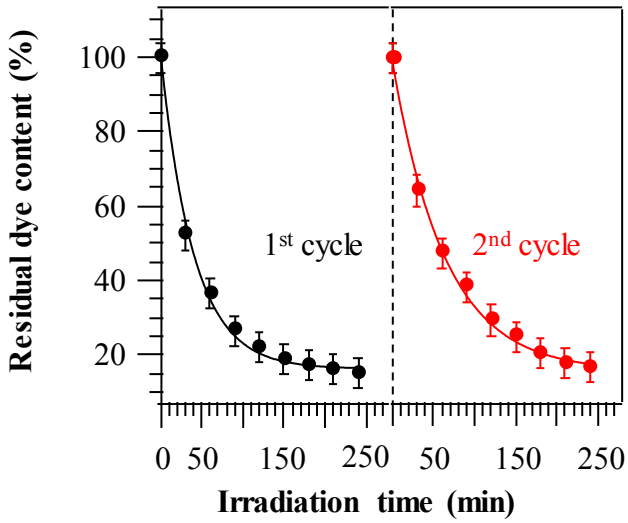

Figure S6. Different UV photodegradation cycles of Plasmocorinth B for a MnO_2 sample fabricated at a growth temperature of 200 °C.

References

1. J. F. Moulder, W. F. Stickle, P. E. Sobol and K. D. Bomben, *Handbook of X-ray Photoelectron Spectroscopy*, Perkin Elmer Corporation, Eden Prairie, MN, USA, 1992.
2. D. Briggs and M. P. Seah, *Practical surface analysis: Auger and X-ray photoelectron spectroscopy*, John Wiley & Sons: New York, 2nd ed., 1990.
3. G. Carraro, A. Gasparotto, C. Maccato and D. Barreca, *Surf. Sci. Spectra*, 2013, **20**, 9-16.
4. K. Saravanakumar, V. Muthuraj and S. Vadivel, *RSC Adv.*, 2016, **6**, 61357-61366.
5. L. Armelao, D. Barreca, G. Bottaro, A. Gasparotto, C. Maccato, C. Maragno, E. Tondello, U. L. Stangar, M. Bergant and D. Mahne, *Nanotechnol.*, 2007, **18**, 375709.
6. N. Kumar, A. Sen, K. Rajendran, R. Rameshbabu, J. Ragupathi, H. A. Therese and T. Maiyalagan, *RSC Adv.*, 2017, **7**, 25041-25053.
7. A. Baral, D. P. Das, M. Minakshi, M. K. Ghosh and D. K. Padhi, *ChemistrySelect*, 2016, **1**, 4277-4285.
8. K. A. M. Ahmed, H. Peng, K. Wu and K. Huang, *Chem. Eng. J.*, 2011, **172**, 531-539.
9. S. Das, A. Samanta and S. Jana, *ACS Sustainable Chem. Eng.*, 2017, **5**, 9086-9094.
10. Y. L. Chan, S. Y. Pung, S. Sreekantan and F. Y. Yeoh, *J Exp Nanosci*, 2016, **11**, 603-618.
11. F. Li, P. Wangyang, A. Zada, M. Humayun, B. Wang and Y. Qu, *Mater. Res. Bull.*, 2016, **84**, 99-104.